Control and Dispatch of Distributed Energy Resources with Improved Frequency Regulation using Fully Active Hybrid Energy Storage System

Aniket Joshi, *Student Member, IEEE,* Arun Suresh, *Student Member, IEEE,* and Sukumar Kamalasadan, *Senior Member, IEEE*

***Abstract*—In this paper a new approach is presented for improving grid inertia based on a Photo-Voltaic (PV) farm in conjunction with a fully active Hybrid Energy Storage System (HESS) comprising of battery and ultra-capacitor. The approach captures grid dynamics using the inverter voltage angle deviation and an error minimization based control is designed for frequency regulation. For this purpose, PV and HESS are integrated at a common DC link that feeds a three phase voltage source inverter (VSI). For demonstration and validation of the proposed approach, a modified IEEE 13 bus and modified IEEE 123 bus power distribution system models are used. It has been observed that the proposed architecture control the Rate of Change of Frequency (RoCoF) and primary frequency and secondary frequency response without the need of frequency-droop information of the system, there by ensuring grid stability that utilize renewable energy based resources.**

***Index Terms*—Micro-grids, Grid Stability, Hybrid Energy Storage Systems, Three Phase Inverter, Grid Inertia.**

I. Introduction

In the process of making PV a reliable source, energy storage systems can contribute for applications such as renewable energy time shift, renewable capacity firming, frequency regulation, energy arbitrage and reactive power support [1], [2]. For the purpose of frequency regulation, energy system can be designed/selected for two distinct operations: Inertial response of grid frequency (primary response) [3], and steady-state frequency regulation (secondary response) [4]. Since inertial response depends on the Rate-of-Change-of-Frequency (RoCoF), it requires storage devices of high power density to supply for a short period of time. However, the secondary regulation, also called droop, requires a device with a high energy density that can supply power in the range of a several minutes up to a few hours. A Hybrid Energy Storage System (HESS) with a combination of battery and ultra-capacitors can be used both for power density and energy density applications. The advantage of HESS is that it can supply a wide range of load demands due to the availability of both high power and high energy density devices in battery and ultra-capacitors [5]. Other methods are either lossy or expensive. For example, high-speed flywheel storage systems exhibit a crucial performance drawback due to higher parasitic losses causing a self-discharge [6], [7] and Super-conducting Magnetic Energy Storage Systems (SMES) are very expensive for discharge period beyond 1 to 2 seconds due to high cost superconducting wires and cooling requirements [8]. Thus UC makes a better option for both inertial and load support as compared to high-speed flywheels and SMES.

DC link topology, considered to study the impact of storage systems gain precedence due to the flexibility of power sharing and ease of integration of Distributed Energy Resources (DERs) into the micro-grid [9]. For frequency regulation, previous work in controller designs include power and phase control (P$-\delta$) [10], where an attempt is made for self-synchronization of $d-q$ inverter. Apart from the advantage of not requiring a phase locked loop (PLL), such approaches still rely on frequency-droop characteristics. Likewise, the control structures of active power-frequency control (P$-\omega$) [11] and reactive power-voltage control (Q$-V$) [12] are heavily dependent on the effective design of DER droop.

Augmented wind turbine control for frequency regulation is discussed in [13], [14] which uses reduced order power grid model. Some of the other works in this direction include, a decentralized droop control strategy on DC micro-grids using virtual admittance method as discussed in [15], and an adaptive control strategy studied in [16] on a 3-phase dq inverter. Two major drawbacks of such architectures are the inefficient energy extraction from PV and non-dispatchable power extraction capability from the inverter. Use of HESS has been demonstrated in [17]. However, the study has only been done in off-grid mode.

In this paper, a grid connected HESS along with a PV farm is proposed for grid frequency regulation based on extended inertia support. The architecture is based on a novel outer loop controller that regulates grid frequency dynamics and at the same time control rate of frequency. The controller works based on voltage angle measurements, thus can be implemented anywhere in the power grid especially on the power distribution network. Other benefits include:

- Frequency regulation can be achieved without requiring the knowledge of micro-grid droop characteristics.
- The architecture performs well during changing grid dynamics and DER intermittency.
- The inertial response and secondary characteristics of grid frequency can be supported by compensating for locally detected voltage angle deviations and it is scalable.

The paper is organized as follows. Section II discusses the design and control of DC micro-grid. Section III discusses the proposed control architecture. The validation of the proposed

This work was supported in part by the NSF grant ECS 1810174, the Energy Production Infrastructure Center (EPIC) and Electrical and Computer Engineering Department at UNC Charlotte.

The authors are with the Energy Production Infrastructure Center (EPIC) and Department of Electrical and Computer Engineering, University of North Carolina at Charlotte, Charlotte, NC 28223 USA. Corresponding Author: S. Kamalasadan (email: skamalas@uncc.edu).

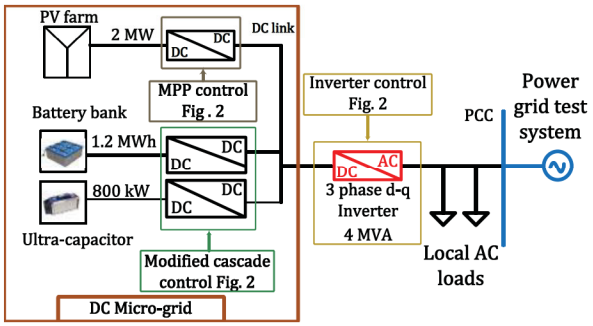

Fig. 1. Proposed DC micro-grid.

micro-grid architecture is performed in section IV. In section V, the scalability of the proposed architecture is evaluated and section VI concludes the paper.

II. Design and Control of Proposed DC Micro-grid

The proposed DC micro-grid comprises of 4 subsystems: PV plant with unidirectional $DC-DC$ converter, battery and ultra-capacitor system with their respective bidirectional $DC-DC$ converters and a three-phase grid connected $d-q$ inverter. The overall system topology is shown in fig 1. Individual control architectures are as follows. DC side of the micro-grid includes PV farm and the HESS comprising of battery and ultra-capacitor system. Each subsystem has its own $DC-DC$ converter as the power conditioning device. The 3-phase grid connected $d-q$ inverter represents the AC side of the micro-grid. The method of controlling converters depends on the type of source used and the control parameter of interest.

A. PV farm control design

For PV, based on the volt−second and capacitor−charge balance equations for the converter the state space representation can be derived as

$$\begin{bmatrix} \dot{\bar{i}} \\ \dot{\bar{V}} \end{bmatrix} = \begin{bmatrix} 0 & \frac{-D'}{L} \\ \frac{D'}{C} & \frac{-1}{RC} \end{bmatrix} \begin{bmatrix} \bar{i} \\ \bar{V} \end{bmatrix} + \begin{bmatrix} \frac{1}{L} & 0 & \frac{V}{L} \\ 0 & \frac{-1}{C} & \frac{i}{C} \end{bmatrix} \begin{bmatrix} \overline{V_{pv}} \\ \overline{i_o} \\ \overline{D_{mpp}} \end{bmatrix} \quad (1)$$

$$\begin{bmatrix} V \\ i \end{bmatrix} = \begin{bmatrix} 0 & 1 \\ 1 & 0 \end{bmatrix} \begin{bmatrix} \bar{i} \\ \bar{V} \end{bmatrix} \quad (2)$$

where $\overline{V_{pv}}$ is the input side Voltage, $\overline{i_o}$ is the output side current and $\overline{D_{mpp}}$ is the duty cycle input to the converter for boost operation, $\bar{i}$, $\overline{V_g}$ and $\overline{V}$ are inductor current, input voltage and output voltage respectively, and the states of the converter. L, C and D' are the inductor, capacitor and the duty cycle for buck operation of the converter.

The control-to-Input voltage transfer function for DC-DC boost converter can be derived as

$$\frac{\overline{V_{pv}}(s)}{\overline{D_{mpp}}(s)} = \frac{(1-D_{mpp})^2 V_o - (1-D_{mpp}) L I_l s}{(LC)s^2 + (\frac{L}{R})s + (1-D_{mpp})^2} \quad (3)$$

where $\overline{V_{pv}}$ is the small signal Input voltage, $\overline{D_{mpp}}$ is the small signal duty cycle, L,C are the DC-DC converter design elements and R is the load resistance. The control architecture on PV farm is shown in fig 2.

B. Inverter control design

The voltage balance equations for an L-type inverter can be written in $d-q$ framework as

$$V_{dl} = L_{inv}\frac{di_d}{dt} - \omega L_{inv} i_q + V_d \quad (4)$$

$$V_{ql} = L_{inv}\frac{di_q}{dt} - \omega L_{inv} i_d + V_q \quad (5)$$

where V_{dl},V_{ql} are d-axis and q-axis voltages across inductor L_{inv}, ω is the angular frequency of the supply voltage, L is the inductance of the L-type filter, i_d, i_q and V_d, V_q are the d-axis and q-axis inverter output current and voltages respectively [18]. Active and reactive power output of the Grid Connected Inverter (GCI) can be given in $d-q$ domain as

$$P = V_d i_d \quad (6)$$

$$Q = V_d i_q \quad (7)$$

Above equations can be represented in state-space as:

$$\begin{bmatrix} \dot{i_d} \\ \dot{i_q} \end{bmatrix} = \begin{bmatrix} 0 & \omega \\ \omega & 0 \end{bmatrix} \begin{bmatrix} i_d \\ i_q \end{bmatrix} + \begin{bmatrix} \frac{1}{L_{inv}} & 0 \\ 0 & \frac{1}{L_{inv}} \end{bmatrix} \begin{bmatrix} (V_{dl} - V_d) \\ (V_{ql} - V_q) \end{bmatrix} \quad (8)$$

$$\begin{bmatrix} P_{ac} \\ Q_{ac} \end{bmatrix} = \begin{bmatrix} V_d & V_q \\ -V_q & V_d \end{bmatrix} \begin{bmatrix} i_d \\ i_q \end{bmatrix} \quad (9)$$

Assuming the grid to be of a constant voltage magnitude we can consider V_d to be a constant. Thus the active and reactive power of the GCI can be controlled by i_d and i_q respectively from (6) and (7). The transfer function of d-axis current ($\overline{i_d}$) versus ($\overline{\Delta V_d}$) can be given in Laplace domain as:

$$\frac{\overline{i_d}(s)}{\overline{\Delta V_d}(s)} = \frac{s}{L_{inv} V_d}\left(\frac{V_d + V_q}{s^2 - \omega^2}\right) \quad (10)$$

where ΔV_d is $V_{dl} - V_d$, s is the Laplace operator.

III. The Proposed Control Architecture

The proposed multi-level control architecture of the DC Micro-grid is shown in fig 2. It consists of a 3-phase $d-q$ inverter primary level control and a hybrid energy storage system secondary level control. **Primary Level Control:** The proposed control structure assigns inverter to regulate the DC bus Voltage of the micro-grid. The inverter control discussed above is applied with an outer loop DC bus Voltage regulation which can be represented by a proportional control gain equal to $\frac{1}{I_{dc}}$, where I_{dc} is the current at the DC bus. To further improve the performance (steady-state error) of this loop an integral controller is also added, thus making the inverter outer loop operate based on a PI-controller. This controller is responsible for DC bus regulation and compensates for the dynamics created by the energy storage power control (secondary level of control) by commanding an active power reference represented in per unit terms as the d-axis current reference (i_d). **Secondary Level Control:** The secondary level control deals with generation of DC power reference based on the inverter voltage angle deviations ($\Delta\delta$). This type of control is popularly know as frequency regulation, involving primary and secondary response characteristics. The proposed approach utilizes error minimization on inverter

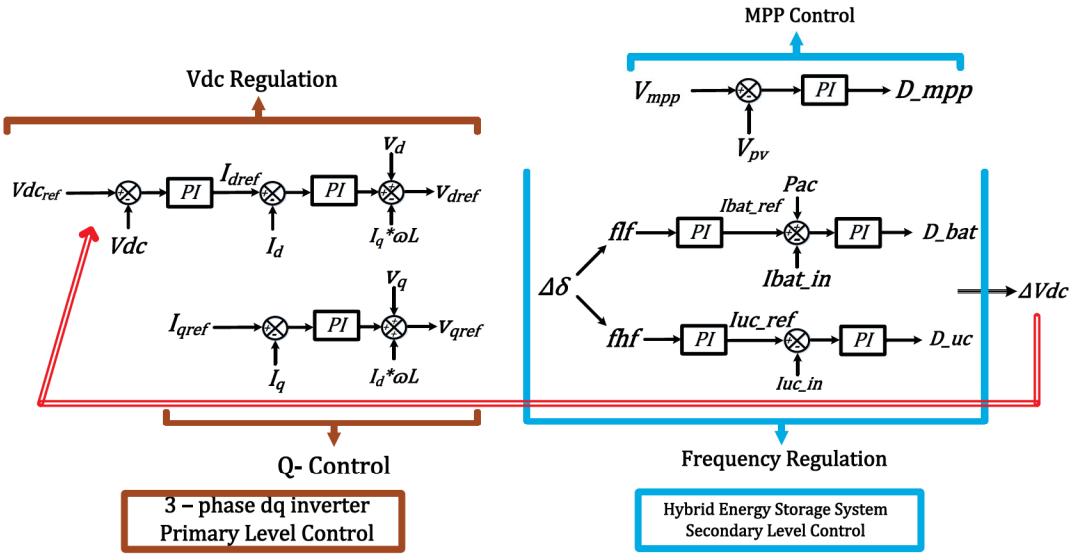

Fig. 2. Proposed Multi-level control structure.

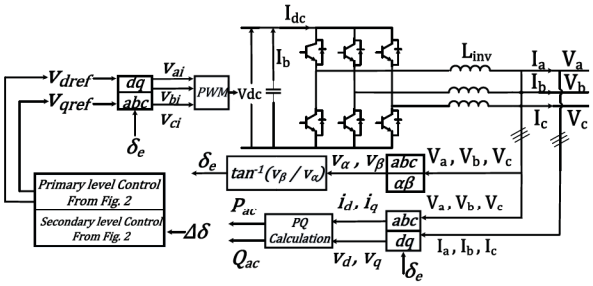

Fig. 3. d-q architecture on 3-phase Inverter

voltage angle deviations which compensates for grid dynamics, thus stabilizing frequency. To arrive at the open loop transfer function it is assumed that the DC-DC converter is lossless and that all the power available at DC bus is converted into equal amount of active power at the inverter output. Thus

$$P_{dc} = P_{bat} \tag{11}$$

$$V_{dc} I_{dc} = V_{bat} I_{bat} \tag{12}$$

$$P_{ac} = P_{dc} \tag{13}$$

where P_{dc} is the power output from battery DC-DC converter at DC bus, P_{bat} is the power input to the DC-DC converter connected to battery source and P_{ac} is the Active Power at the inverter output, V_{dc} is the DC bus Voltage, I_{dc} is the DC bus current, V_{bat} is the input-side converter Voltage (battery terminal voltage) and I_{bat} is the input-side converter current (battery terminal current). Also, the power transfer through an inductive line, assuming $sin(\delta) \approx \delta$ can be written as

$$P_{ac} = \frac{V_1 V_2 \delta}{X} \tag{14}$$

where P_{ac} is the 3-phase AC Active Power, V_1 is the sending end Voltage, V_2 is the receiving end Voltage, δ is the Voltage angle difference between V_1 and V_2 and X is the inductive reactance between the sending and receiving end.

The state space representation of the DC-DC boost converter discussed in Section II-A gives us the relationship between output-side voltage and input-side current,

$$\frac{V_{dc}(s)}{I_{bat}(s)} = \frac{s\frac{I_{in}}{C} - \frac{V_{dc}D'}{L}}{s\frac{V_{dc}}{L} + \frac{V_{dc}}{RLC} + \frac{I_{in}D'}{C^2}} \tag{15}$$

Using equations (11), (12), (13), (14) and (15) we arrive at the following equation:

$$\frac{\Delta\delta(s)}{Ibat\_ref(s)} = \frac{s\frac{X I_{dc} I_{in}}{C} + \frac{P_{dc} X D'}{L}}{s\frac{V_{dc} V_1 V_2}{L} + \frac{V_{dc} V_1 V_2}{RLC} + \frac{I_{in} D' V_1 V_2}{C^2}} \tag{16}$$

where $Ibat\_ref$ is battery current reference and shown in fig 2, $\Delta\delta(s)$ synthesis can be found in fig 4. The open loop transfer function derived in equation (16) represents the uncompensated plant for the secondary level control in our micro-grid. This loop regulates the voltage angle difference at the point of common coupling of the micro-grid. The δ is directly linked with the grid angular frequency (ω) by the following equation:

$$\delta = \int \omega dt \tag{17}$$

The objective of the outer loop is to minimize the rate of change of $\Delta\delta$ ($\frac{\Delta(\Delta\delta)}{\Delta t} = \frac{d\Delta\delta}{dt}$). This is seen as error by the outer loop. The error signal is sent through a low pass filter to obtain a low frequency error signal (flf). The high frequency signal (fhf) is derived from the difference in total error and flf shown in fig 4.

$$\Delta\delta = \delta_e - \delta_{pcc} \tag{18}$$

TABLE I
CONTROLLER GAINS AFTER DESIGN AND TUNING

Control Loop	k_p	k_i
$\Delta\delta$ (frequency regulation)	146.87	56.73
HESS Current/Power	1.3	3
Inverter d-axis current/Active Power	0.86	0.6
Inverter q-axis current/Reactive Power	-0.86	-0.6
PV MPPT	-1.5	-7

$$\frac{d\Delta\delta}{dt} = flf + fhf \tag{19}$$

where δ_{pcc} is the voltage angle at PCC, δ_e is the Voltage angle at the inverter output, $\Delta\delta$ is the angle difference between inverter voltage and PCC voltage, flf is the low frequency error signal and fhf is the high frequency error signal.

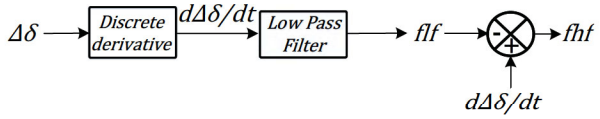

Fig. 4. High and low frequency error signal generation in p.u.

The summary of the secondary level control is shown in fig 2, where the high frequency error is scheduled to UC source and the slow changes in error are referenced to the battery. In addition to that, the battery is also made responsible for active power load demands from the AC side, as we know that DC power gets converted into equivalent AC power at inverter output. This is represented by the term P_{ac} in fig 2. The use of per unit controllers make it possible to represent power references as current. The closed loop control on energy storage system allows power regulation on the DC side of the micro-grid. However, the power references commanded by secondary level controllers will induce dynamics on the DC bus in terms of voltage wobble which is regulated by the primary level control discussed in section II-B.

The summary of the multi-level control structure is given by loop gain as shown in equation (20).

$$G(s) = \frac{\delta(s)}{Ibat(s)} * \frac{Ibat(s)}{d(s)} * \frac{d(s)}{Vdc(s)} * \frac{Vdc(s)}{i_d(s)} * \frac{i_d(s)}{\Delta V_d(s)} \tag{20}$$

where $\frac{Vdc(s)}{i_d(s)} * \frac{i_d(s)}{\Delta V_d(s)}$ represents the inverter d-q control (primary level), $\frac{Ibat(s)}{d(s)}$ is the battery current control applied on the DC micro-grid, $\frac{d(s)}{Vdc(s)}$ represents the effect of input side current control on DC bus voltage and $\frac{\delta(s)}{Ibat(s)}$ describes the gain for the frequency regulation loop (secondary level) which gives a battery current reference. The control design is summarized in the Table I.

IV. PROOF-OF-CONCEPT STUDY

For this work a modified IEEE 13 bus system, involving a micro-grid and a synchronous generator model as a source is used for proof-of-concept study. The synchronous generator is added with a governor control to emulate the basic inertial response of the generator to fault or power mismatch. Micro-grid structure is integrated at bus 634. Fig 5 shows the modified IEEE 13 bus system and the Point of Common Coupling (PCC) for micro-grid. Bus 634 of the modified test system operates at 480V which makes micro-grid integration favorable. GCI is designed for 4 MVA rating and operates at 480V at its output.

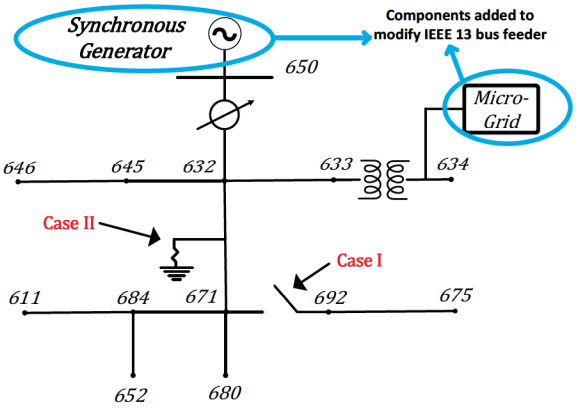

Fig. 5. Modified IEEE 13 bus system with micro-grid and synchronous generator model.

A. Case Studies on the Modified 13 Bus System

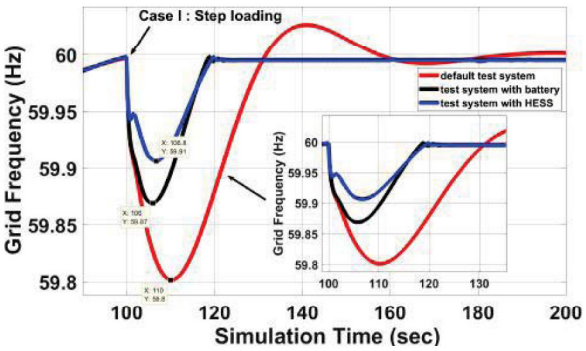

Fig. 6. Case I : Frequency regulation for (800 kW / 10%) Step loading @ 100s.

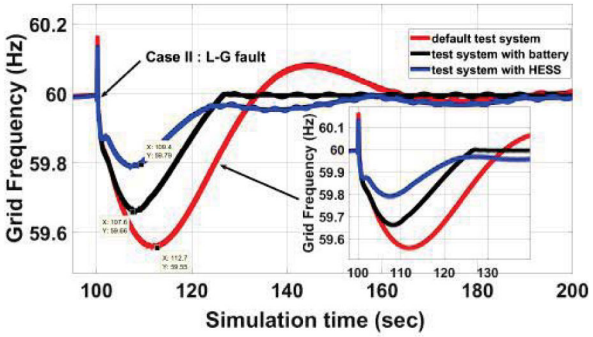

Fig. 7. Case II : Primary and secondary frequency response for the system.

1) Frequency response to Step loading (Case I): Fig 6 showcases the primary and secondary response of the system for step loading at bus 671 on the modified 13 bus system. When a 10% step change in load is injected into the system the frequency nadir reaches 59.8 Hz for the modified 13 bus system with SGC generator. The secondary response takes about 166 seconds to settle. When the micro-grid brings in BESS for frequency regulation, the frequency nadir improves to 59.87 Hz. A performance comparison between HESS and BESS is presented in Table II which clearly shows the contribution of UC in reducing the frequency nadir.

2) Frequency response to L-G Fault (Case II): The severity of L-G fault on power grid is evident in Fig 7, where the frequency nadir is seen dropping as low as 59.55 Hz for the modified 13 bus system. Addition of HESS slightly improves frequency to 59.79 Hz as opposed to 59.66 Hz for BESS case. The settling time for the modified 13 bus system is around 183 seconds compared to 160 seconds after HESS addition. BESS case frequency settles the earliest at about 125 seconds. Table II summarizes the case study performed on the modified 13 bus system. The following abbreviations are used during the formulation of the table and also apply to Table III: MBS is Modified Bus System; Imp Vs MBS is Improvement Versus Modified Bus System.

V. Scalability Study

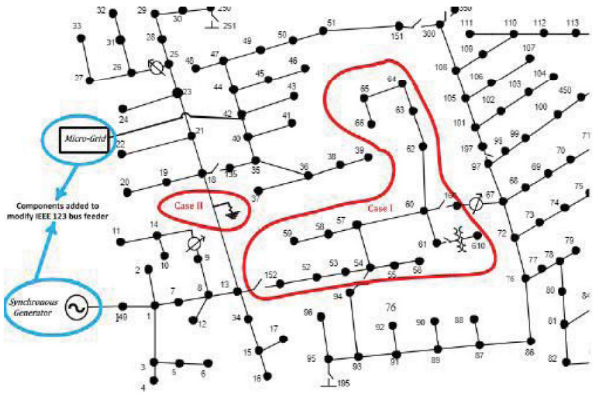

Fig. 8. Micro-grid integration study for a 123 bus feeder.

The scalability of the proposed structure is tested using an IEEE 123 bus feeder [19]. Feeder is modified by adding a synchronous generator at bus 149 and micro-grid integration at bus 42. Cases I and II discussed in IV-A are performed again on this system to validate scalability. To execute Case I lines between 13 and 152 are closed at 100 seconds, thus adding 550 kW of unbalanced loads. The L-G fault in the modified 123 bus system is introduced at bus 18 and the response is recorded under Case II. Fig 8 shows test cases I and II performed on the modified 123 bus system.

A. Frequency response to Step loading (Case I)

Fig 9 presents frequency curves for step loading for the modified 123 bus system. As seen from the figure the system frequency drops to 59.82 Hz. Improvements in frequency

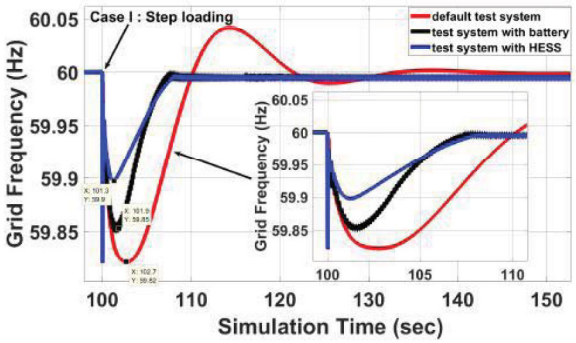

Fig. 9. Case I : Frequency regulation for (550 kW / 6.8%) Step loading @ 100s.

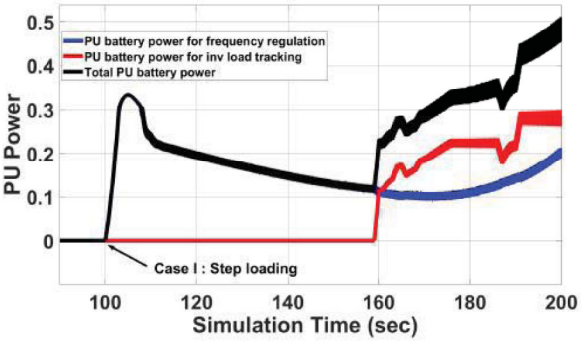

Fig. 10. Case I : PU battery power sharing for frequency regulation and inverter load tracking (900 kW base).

nadir are observed after inclusion of BESS and HESS systems through micro-grid, 59.85 Hz and 59.9 Hz respectively. Settling time for the modified 123 bus system is 150 seconds, whereas BESS and HESS cases settle as early as 109 seconds. Fig 10 proves that battery storage size is enough to provide support for step loading dynamics along with load changes.

B. Frequency response to L-G Fault (Case II)

Similar to the modified 13 bus system, the modified 123 bus system frequency is affected more severely due to a L-G fault. The frequency nadir drops to 59.5 Hz. As shown in fig 11, BESS case performs slightly better with frequency nadir at 59.54 Hz and addition of HESS again allows frequency to drop the least with 59.71 Hz. However, in contrast to case results in IV-A2, introduction of HESS system shows the fastest settling time at 122 seconds compared to 140 seconds for BESS incorporation and 165 seconds with the modified 123 bus system. Table III showcases the result for the modified 123 bus system. The medium size test system performs well under both cases with introduction of HESS into the system. The frequency regulation improves by more than 40% in both step loading and L-G fault with faster settling time.

VI. Conclusions

This paper presents a new control architecture for grid frequency regulation and validates its implementation and scalability on modified IEEE 13 and 123 bus systems respectively.

TABLE II
RESULTS ON MODIFIED 13 BUS SYSTEM

	Parameter	MBS	MBS + battery	Imp Vs MBS	MBS + HESS	Imp Vs MBS
Case I	Frequency Nadir (Hz)	59.8	59.87	35%	59.91	55%
	Settling time (s)	166	125	41	125	41
Case II	Frequency Nadir (Hz)	59.55	59.66	24.45%	59.79	53.33%
	Settling time (s)	183	125	58	160	23

TABLE III
RESULTS ON MODIFIED 123 BUS SYSTEM

	Parameter	MBS	MBS + battery	Imp Vs MBS	MBS + HESS	Imp Vs MBS
Case I	Frequency Nadir (Hz)	59.82	59.85	16.67%	59.9	44.45%
	Settling time (s)	150	109	41	109	41
Case II	Frequency Nadir (Hz)	59.5	59.54	8%	59.71	42%
	Settling time (s)	165	140	25	122	43

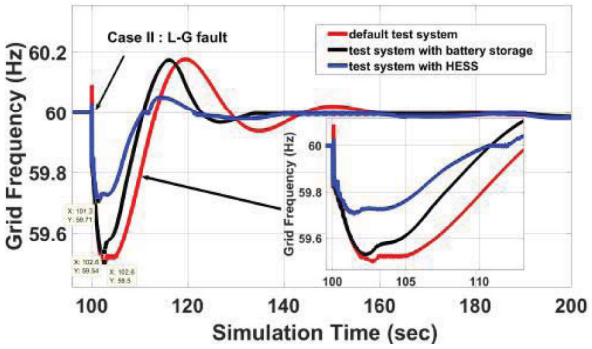

Fig. 11. Case II : Primary and secondary frequency response for the system.

The proposed DER control topology enables dispatch-able operation of DC microgrids using a 3-phase load following GCI for improved inertial and secondary frequency response without the need of frequency-droop information of the system. Such architecture is favorable for DERs connected in DC link topology as it aims at regulating the grid frequency locally and independent of the dynamics introduced by other micro-grids in the network.

REFERENCES

[1] J. Eyer and G. Corey, "Energy storage for the electricity grid: Benefits and market potential assessment guide."

[2] S. A. Abdelrazek and S. Kamalasadan, "Integrated pv capacity firming and energy time shift battery energy storage management using energy-oriented optimization," *IEEE Transactions on Industry Applications*, vol. 52, no. 3, pp. 2607–2617, May 2016.

[3] D. Chen, Y. Xu, and A. Q. Huang, "Integration of dc microgrids as virtual synchronous machines into the ac grid," *IEEE Transactions on Industrial Electronics*, vol. 64, no. 9, pp. 7455–7466, Sep. 2017.

[4] J. Fang, Y. Tang, H. Li, and X. Li, "A battery/ultracapacitor hybrid energy storage system for implementing the power management of virtual synchronous generators," *IEEE Transactions on Power Electronics*, vol. 33, no. 4, pp. 2820–2824, April 2018.

[5] G. Deshpande and S. Kamalasadan, "An approach for micro grid management with hybrid energy storage system using batteries and ultra capacitors," in *2014 IEEE PES General Meeting — Conference Exposition*, July 2014, pp. 1–5.

[6] J. W. Kimball, B. T. Kuhn, and R. S. Balog, "A system design approach for unattended solar energy harvesting supply," *IEEE Transactions on Power Electronics*, vol. 24, no. 4, pp. 952–962, April 2009.

[7] A. Burke, "Ultracapacitors: why, how, and where is the technology," *Journal of Power Sources*, vol. 91, no. 1, pp. 37 – 50, 2000. [Online]. Available: http://www.sciencedirect.com/science/article/pii/S0378775300004857

[8] M. Farhadi and O. Mohammed, "Energy storage technologies for high-power applications," *IEEE Transactions on Industry Applications*, vol. 52, no. 3, pp. 1953–1961, May 2016.

[9] P. Cairoli and R. A. Dougal, "New horizons in dc shipboard power systems: New fault protection strategies are essential to the adoption of dc power systems." *IEEE Electrification Magazine*, vol. 1, no. 2, pp. 38–45, Dec 2013.

[10] Y.Kimpara, M.Kurimoto, and T. Y.Manabe, "An experimental study on active power control of photovoltaic power generation for supporting grid frequency regulation," in *2018 IEEE Power Energy Society General Meeting (PESGM)*, Aug 2018, pp. 1–5.

[11] Y. A. I. Mohamed and E. F. El-Saadany, "Adaptive decentralized droop controller to preserve power sharing stability of paralleled inverters in distributed generation microgrids," *IEEE Transactions on Power Electronics*, vol. 23, no. 6, pp. 2806–2816, Nov 2008.

[12] A. Wang and J. Zhang, "A novel reactive power control strategy in virtual flux droop control," in *2017 18th International Symposium on Electromagnetic Fields in Mechatronics, Electrical and Electronic Engineering (ISEF) Book of Abstracts*, Sep. 2017, pp. 1–2.

[13] A. Thakallapelli and S. Kamalasadan, "An online reduced order modeling based frequency regulation adaptive control architecture for wind integrated power grid," in *2018 IEEE Industry Applications Society Annual Meeting (IAS)*, Sep. 2018, pp. 1–8.

[14] S. Ghosh, S. Kamalasadan, N. Senroy, and J. Enslin, "Doubly fed induction generator (dfig)-based wind farm control framework for primary frequency and inertial response application," *IEEE Transactions on Power Systems*, vol. 31, no. 3, pp. 1861–1871, May 2016.

[15] S. Yana, A. F. James, A. Emhemed, and G. Burt, "Decentralised control of dc microgrid based on virtual admittance to enhance dc voltage and grid frequency support," in *2018 53rd International Universities Power Engineering Conference (UPEC)*, Sep. 2018, pp. 1–6.

[16] R. Bhattarai, N. Gurung, and S. Kamalasadan, "Dual mode control of a three-phase inverter using minimum variance adaptive architecture," *IEEE Transactions on Industry Applications*, vol. 54, no. 4, pp. 3868–3880, July 2018.

[17] J. Fang, X. Li, Y. Tang, and H. Li, "Power management of virtual synchronous generators through using hybrid energy storage systems," in *2018 IEEE Applied Power Electronics Conference and Exposition (APEC)*, March 2018, pp. 1407–1411.

[18] M. Davari and Y. A. I. Mohamed, "Robust vector control of a very weak-grid-connected voltage-source converter considering the phase-locked loop dynamics," *IEEE Transactions on Power Electronics*, vol. 32, no. 2, pp. 977–994, Feb 2017.

[19] W. H. Kersting, "Radial distribution test feeders," in *2001 IEEE Power Engineering Society Winter Meeting. Conference Proceedings (Cat. No.01CH37194)*, vol. 2, Jan 2001, pp. 908–912 vol.2.